I J C T A, 9(5), 2016, pp. 2111-2127

Performance Analysis of a Wind Duct and SOC Estimation for Pure Electric Vehicle Charging

Chellaswamy C.*, and Ramesh R.**

ABSTRACT

Electric vehicles (EVs) are noise less, pollutants free but require frequent charging. The countries which uses EVs provides electricity charging facility through the road side stations, shopping complexes, and parking areas for charging EVs. This way of charging provides an incredible increase in the travel time and new investment. To overcome this difficulty we have proposed a new green energy harvesting (GEH) system for charging EVs. GEH automatically energize the battery packs present in the EV and the control mechanism is used to avoid the need for driver involvement. The system has a rectangular wind duct connected with the drive train assembly integrated with a control system. The main focus of this recharging system is to reduce the travelling time and increase the usage of EVs. In this study, we are mainly focusing the performance of the rectangular wind duct for various speed scenario of the vehicle. Moreover, for estimating the state of charge (SOC), available power of the battery pack we introduced unscented Kalman filter (UKF). Simulation results show that the axial and rotational boundary layer thickness depends on the duct angle, the velocity ratio, and Reynolds number. The performance of UKF was compared with the extended Kalman filtering (EKF) and the result shows that UKF produces less error than EKF and it can be suitable for EV applications.

Keywords: electric vehicle, rectangular duct, extended Kalman filter, state of charge, uncended Kalman filter

1. INTRODUCTION

There is an ever-ending demand for fossil fuel, population rise and demand for vehicles. Hence, this has turned our concern towards the excess emission of greenhouse gases. This has been demanded for a research on electric vehicles, which are much more eco-friendly. These vehicles are used to reduce the dependence on fossil fuels since 1990s, their penetration into the market has not been high enough because these vehicles are not so cost effective and it recharges the batteries once in 60 km or 70 km depends on the capacity of EVs. Present market consists of hybrid vehicles deriving their energy from the combustion engines. However in order to mitigate the gasoline consumption, the plug-in electric vehicles have been introduced in the market, which can take energy from the grid. These vehicles are still under research for its improvements on battery-life, costs and grid connection. Electric vehicles produce very less pollution and the frequency of usage of EVs is reduced due to the present recharging system. Nowadays EVs gets charged through roadside units, park stations, and in homes. For recharging the storage system present in the EV takes couple of hours based on the capacity and it will increase the travelling time, thus it limitsthe vehicle usage. To overcome this difficulty, an automatic recharging mechanism is introduced [1]. The control mechanism automatically charges the storage system without the involvement of the driver. The performance of the system was studied and comparison of CO_2 emission for different vehicle has been studied. The EVs

* Research Scholar, St. Peter's University, St. Peter's Institute of Higher Education and Research, Chennai, India, *Email: chella_info@yahoo.co.in*

** Professor, Department of Electronics and Communication Engg., Saveetha Engineering College, Chennai, India, *Email: ramesh@saveetha.ac.in*

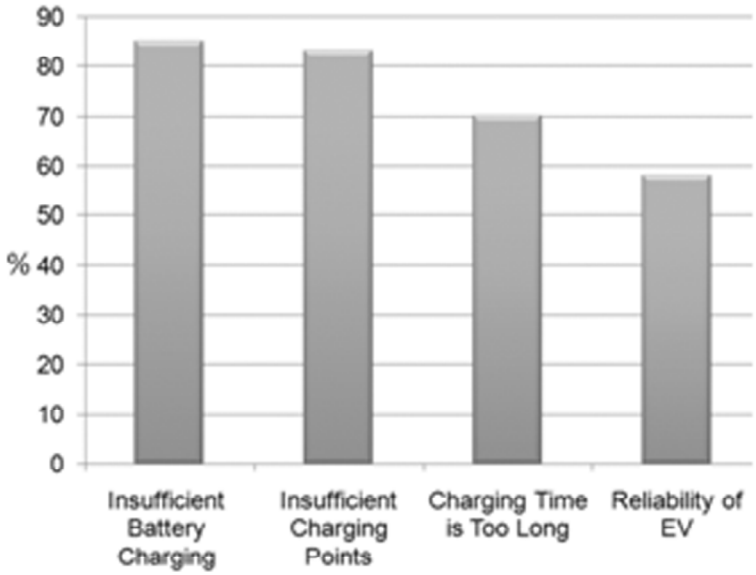

Figure 1: Factors affecting to purchase full EV [9].

need to meet the recharging infrastructure frequently for charging the storage system. A new system is introduced to find the location, payment, and future enhancements were studied [2]. It consists of different features like location privacy, catching fraudulent statement, slandering, and hiding. To reduce greenhouse gas emission utilization of EVs are very important and interfacing EVs to micro grid are popular for recharging [3]. An optimal control and scheduling mechanism, which controls the electricity consumption of both the home appliances and EVs is necessary. The mixed integer linear programming is used to solve the scheduling problem optimally. The operating cost and CO_2 emission of a hybrid EV is calculated under the European regulations [4]. A global optimization algorithm is developed for minimizing the CO_2 emission of EVs. The cost analysis of battery discharge has been done and compared with the cost of engine for satisfying the customers and increase the frequency of EVs. A new formulation of artificial dissipation coefficient required for Navier-Stokes in turbulent boundary layer estimation and scaling functions are used by Shalman et al. [5]. This scaling provides damping in the estimation of boundary layer and a coarse grid is used for getting greater accuracy. For calculating the boundary layer thickness a transonic flow over a NACA airfoil is used.

The grid, which is used here, produces more accuracy in estimating the boundary layer computation. A turbulent flow modeling use high resolution Reynolds Navier-Stokes method for analyzing 3-D building arrays. Two different models were tested and the turbulent kinematic energy and viscous dissipation rate are estimated [6]. They used standard and Kato-Launder models to predict the turbulence kinetic energy around the stagnation point. The stress present in point to point flow related to the Reynolds stress has been calculated for the building array. A three dimensional axisymmetric Navier-Stokes model is studied to avoid tremendous dynamic growth of one dimensional model. Thomas and Congming applied this method and get dynamic depletion mechanism, which prevent the outcome in a short duration of time [7]. This estimation produces large dynamic growth even though the overall solution is accurate and smooth.

The environmental electrification of ships is important and become popular. Optimal energy management system plays a major role to reduce the fuel consumption [8]. A full electric system for the ship propulsion and storage system reduces the total energy consumption. A global survey has been done for plug-in electric vehicles (PEV). The customer preferences and opinion about PEV and charging services has been done for 13 countries [9]. Analysis of different factors affecting purchase of EV is shown in figure 1. Green energy sources produces fluctuating electric power and it can be stored in a storage system for further usage. Cascaded pulse width modulation for balancing the state of charge of battery packs are studied by Laxman et al. [10]. Nine NiMH batteries are used for balancing SOC and a control algorithm is introduced for

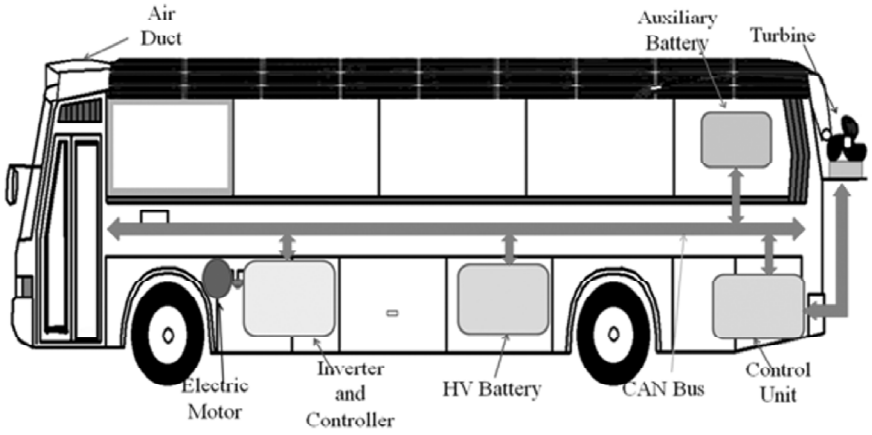

Figure 2: Arrangement of wind duct on the top of vehicle with other devices.

making the SOC equal to all the batteries. Analysis of battery SOC variation for different temperature has been studied and a model is developed for improving the SOC estimation [11]. The performance of first order RC network model is compared with the open circuit voltage with temperature variation and a new set of data is generated and replaced the old one.

A comparative analysis has been done for SOC with temperature and better result has been achieved. A parking garage is used to electrifying the plug-in EVs [12]. A smart algorithm is introduced for the controller, to limit the charging rate and to reduce the cost of charging. SOC estimation is complex and it is important to improve the increase usage of EVs. A new robust EKF is introduced to estimate lithium-ion battery. An improved lumped circuit model has been implemented based on generic algorithm [13]. The analysis has been performed using urban driving schedule and the simulation result shows that the battery model produces better accuracy. The robust EKF method eliminates the accumulation of calculation problems and the initial state estimation error. An integral charger for the battery packs present in the electric scooter with power factor correction capability using fixed point DSP (digital signal processing) controller [14]. In this method no additional filtering is needed because pulse width modulation is used for minimizing the ripple. A control algorithm is developed for a power factor correction boost rectifier prototype and tested in the scooter [15].

The battery is a non-linear system so that an extended version of Kalman filter called extended Kalman filtering (EKF) is used for estimating different parameters of battery. Compared with particle filter (PF) the EKF has less computational complexity. A battery model is constructed using a second order RC network and the open circuit voltage is measured in the lithium ion phosphate battery for estimating the SOC for EVs. The load characteristic of the second order network has been analyzed [16]. A recursive Kalman filter is used for the calibration process and an algorithm is realized in the recursive form. The calibrations are studied under different conditions. For calculating the state estimation of non linear system unscented Kalman filtering (UKF) is used instead of EKF [17]. Comparing the performance of UKF with EKF four different cases has been studied and the UKF is better than EKF in terms of speed of convergence and robustness. Another method for estimating non-linear states, a constrained EKF is introduced and the dynamic states are considered as algebraic equality or inequality constraints [18]. The constrained EKF can be computed with little additional computational cost. The EKF which is used for non-linear estimation is difficult to tune, difficult to implement, reliable for almost linear system, and arises linearization problems [19].

To overcome these difficulties an unscented transformation was developed and it provides accurate results and easy to implement. It can be used in high nonlinear control applications. Recursive bayesian estimation based optimal EKF is used to estimate the nonlinear system parameters [20]. The derivative less

Table 1
Top electric vehicles and its various ratings.

Name of EV	*Battery Type*	*Capacity*	*Range*	*Charge Time*	*Charging Voltage/Current*
BMW Mini E	Lithium ion with Air cooled.	35 kWh	96 miles	26 hours 4.5 hours 3 hours	110V/12 amp 240V/32amp 240V/48 amp
Chevy Volt	Liquid cooled Lithium managanese cells from Lg Chem.	16kWh	40 miles	10 hours 4 hours	120V/12amp 240V/24amp
Ford Focus EV	Lithium ion tri-metal cells from LG Chem.	23kWh	75 miles	6-8 hours	230V/32amp
Smart Fortwo ED	Lithium ion	16.5kWh	85 miles	3.5-8 hours	220V/24 amp
Tesla Model S	Standard (larger premium batteries optional)	42kWh	160 miles	3-5 hours	220V/70 amp
Tesla Roadster	Lithium cobalt Liquid cooled.	56kWh	220 miles	3.5 hours	220V/70amp
Think City	Lithium ion batteries	24.5kWh	99 miles	8 hours	110V/48 amp
Volvo Electric C30	Lithium ion batteries	24 kWh	93 mile	8 hours	230V/16 amp

deterministic algorithm called sigma point Kalman filter are used to study machine learning problems and it can be used where EKF is not possible to estimates.

The EVs used in different countries and its various ratings are shown in table 1. The charging time required for EVs are depends upon the power rating (ie: multiplication of current and voltage) of the input. According to table 1 the minimum charging is required for full charging of EV and it is around 3-4 hours. Huge variation can be observed in the travelling time for long distance. Most of the developed countries have used EVs for creating green environment. The arrangement of wind duct incorporated with other devices is shown in figure 2. We extend the work based on the previous work [1]. The remainder of this paper is organized as follows: section 2 describes the overview of proposed system; section 3 describes flow analysis of rectangular duct; section 4 explains the UKF; section 5 explains the simulation results of both the wind duct and SOC of battery; and finally, conclusion is discussed in section 6.

2. SYSTEM DESCRIPTION

The vehicle which runs through fuel produces more greenhouse emission and pumped into atmosphere. The cost is increasing everyday for controlling the pollution. Green energy utilization in EVs becomes popular to reduce the pollutants produced by fuel vehicles. The major disadvantage of EV is storage of energy and distance to be travelled for the same charge. This study mainly focused to solve this problem.

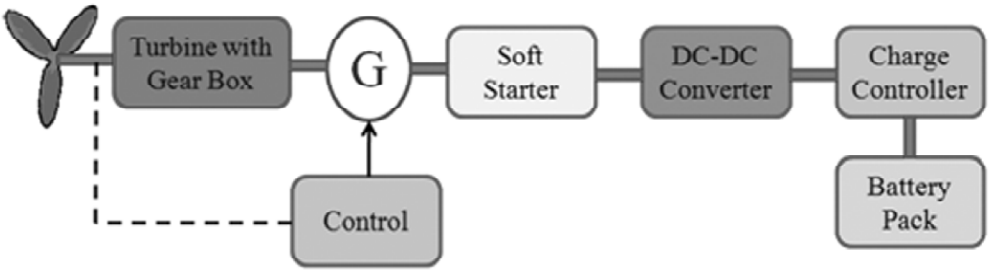

Figure 3: Block diagram of proposed system.

GEH automatically charge the battery packs present in the EVs. The advanced permanent magnet synchronous generator (PMSG) and the drive systems are used for producing power. The ARM-7 based controller with sensing system is communicated through controller area network (CAN). A high power converter is used for fast charging of storage system present in the EVs.

A turbine with gear arrangement is connected with a variable speed PMSG. If the vehicle is moving, PMSG generates power and it is proportional to the speed of the vehicle. A variable speed wind turbine is used to increase the power quality and reduce the mechanical stress. The battery management system is interfaced with the sealed battery packs via CAN bus communication. It also measures the battery SOC, and power under running condition. The block diagram of proposed system is shown in figure 3. The SOC represents the amount of energy contains in the battery and it should be maintained between 20% and 95%. The controller always senses the SOC and maintains 20<SOC<95. The advantages of GEH are given below:

1. Energize the battery pack through green energy harvesting leads to eliminate pollutants.
2. Recharging stations are not required for charging the battery packs of EV.
3. Compared to EV the proposed system (GEH) reduces the travelling time.
4. GEH overcome the future fuel crisis.

In this study, we concentrate two major areas such as 1) performance of wind duct 2) SOC estimation. The flow characteristics of wind duct such as boundary layer thickness, shear stress, and effect of Reynolds number (RN) has been analyzed. In a constant cross section in both the end of the pipe has negative pressure gradient due to increase of boundary layer. If the cross sectional area is reduced the rotational velocity increases along with the stream wise direction. These results in the development of boundary layer or it will be reduced.

To estimate the real time SOC we use UKF. For this estimation, a non-linear transformation is used for estimating the random variables which is used to calculate SOC. A wind duct is constructed on the top of the EV. The shape of the wind duct is like a rectangular cone, i.e. the outlet mouth is slowly reducing. An

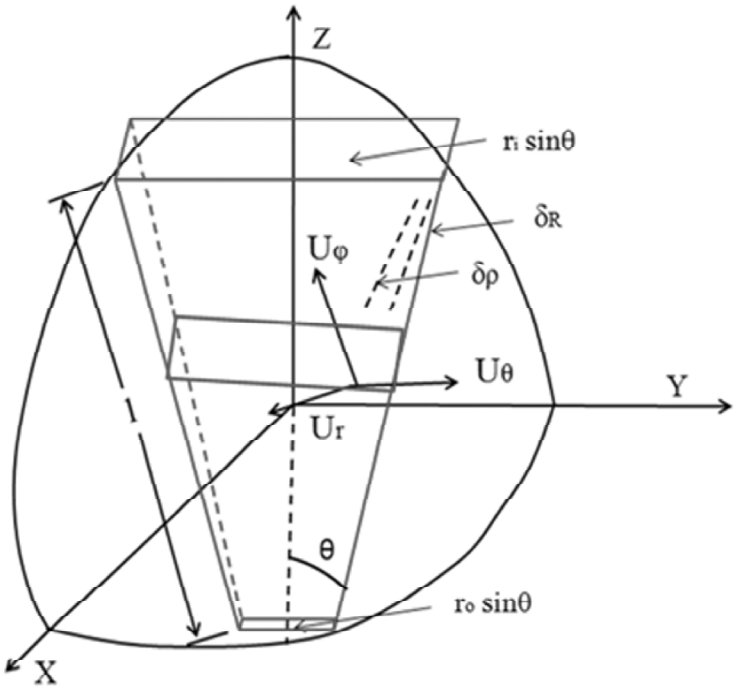

Figure 4: Rectangular duct in a spherical coordinate.

automatic opening valve is incorporated at the end of the duct to release the pressure higher than the allowable pressure.

3. FLOW ANALYSIS OF DUCT

The complex features of turbulent flow wind duct are calculated by using Navier-Stocks equation. The turbulent fluctuation produces non-normality, rapid growth disturbance energy, and non-linearity. The lifetime of turbulence is finite near the edge of the revolution [26]. Numerous experiments have been studied by Eckhardt et al. [25] for the importance of turbulent fluctuation inside the duct. There is a weak connection between the chaotic flow and the flow structure grows during linear transient phase. In this study we assume that the dynamic flow of air free vertex velocity profile and its velocity depend on the speed of vehicle. The boundary layer assumptions are applied in Navier-Stocks equation and the turbulent flow parameters of convergent wind duct such as shear stress, the boundary layer growth, and the effect of RN.

The spherical coordinate system can be built upon three mutually perpendicular axes *x*, *y*, and *z* with radial displacement (*r*) and two angular displacements (θ and φ). The wind velocity is proportional to the speed of the vehicle. The length of the duct is l, height is h, and the inside velocity of boundary layer for the three directions are *Ur*, *U*θ, *U*φ. The suffix '*i*' indicates the inlet, '*o*' indicates the outlet of the duct and *s* represents the outer surface of the wind duct. The incremental area of the surface of sphere is dA. The wind duct is placed in the spherical coordinate system is shown in figure 4. The wind duct is considered as an axisymmetric convergent nozzle and the Navier-Stokes equation related to incompressible flow for spherical coordinate system as [24].

$$\rho\left(U_r\frac{\partial U_r}{\partial r}+\frac{U_\theta}{r}\frac{\partial U_r}{\partial\theta}-\frac{U_\varphi^2+U_\theta^2}{r}\right)=-\frac{\partial p}{\partial r}+\eta\begin{matrix}\frac{1}{r^2}\frac{\partial^2U_r}{\partial\theta^2}+\frac{1}{r^2}\frac{\partial^2\left(r^2U_r\right)}{\partial\theta^2}+\\ \frac{\cot\theta}{r^2}\frac{\partial U_r}{\partial\theta}\end{matrix} \tag{1}$$

$$\rho\left(U_r\frac{\partial U_\theta}{\partial r}+\frac{U_\theta}{r}\frac{\partial U_\theta}{\partial\theta}+\frac{U_rU_\theta}{r}-\frac{U_\varphi^2\cot\theta}{r}\right)=-\frac{\partial p}{r\partial\theta}+\eta$$
$$\left[\frac{1}{r^2}\frac{\partial}{\partial r}\left(r^2\frac{\partial U_\theta}{\partial r}\right)+\frac{1}{r^2}\frac{\partial}{\partial\theta}\left(\frac{1}{\sin\theta}\frac{\partial}{\partial\theta}(U_\theta\sin\theta)\right)+\frac{2}{r^2}\frac{\partial U_r}{\partial\theta}\right] \tag{2}$$

$$U_r\frac{\partial U_\varphi}{\partial r}+\frac{U_\theta}{r}\frac{\partial U_\varphi}{\partial\theta}+\frac{U_rU_\varphi}{r}-\frac{U_\varphi U_\theta\cot\theta}{r}=\frac{\eta}{\rho}$$
$$\left[\frac{1}{r^2}\frac{\partial^2U_\varphi}{\partial\theta^2}+\frac{1}{r^2}\frac{\partial}{\partial r}\left(r^2\frac{\partial U_\varphi}{\partial r}\right)+\frac{\cot\theta}{r^2}\frac{\partial U_\varphi}{\partial\theta}+\frac{2}{r^2}\frac{\partial U_r}{\partial\theta}+\frac{U_\varphi}{r^2}\frac{-(1+\tan^2\theta)}{\tan^2\theta}\right] \tag{3}$$

$$\frac{1}{r^2}\frac{\partial}{\partial r}(r^2U_r)=-\frac{1}{r\sin\theta}\frac{\partial}{\partial\theta}(U_\theta\sin\theta) \tag{4}$$

The following boundary layer approximations $U_r = U_\theta$, $\frac{\partial^2}{\partial\theta^2} >> \frac{\partial^2}{\partial r^2}$, $\frac{\partial}{\partial\varphi} = 0$, $U_\theta = 0$ can be applied for the axisymmetric wind duct and the above equations can be reduced as follows:

$$U_r \frac{\partial U_r}{\partial r} + \frac{U_\theta}{r}\frac{\partial U_r}{\partial \theta} - \frac{U_\varphi^2}{r} = -\frac{1}{\rho}\left[\frac{\partial p}{\partial r} + \eta\left(\frac{1}{r^2}\frac{\partial^2 U_r}{\partial \theta^2}\right)\right] \tag{5}$$

$$-\frac{U_\varphi^2}{r}\cot\theta = -\frac{1}{\rho r}\frac{\partial p}{\partial \theta} \tag{6}$$

$$U_r \frac{\partial U_\varphi}{\partial r} + \frac{U_\theta}{r}\frac{\partial U_\varphi}{\partial \theta} - \frac{U_\varphi U_r}{r} = \frac{\eta}{\rho}\left(\frac{1}{r^2}\frac{\partial^2 U_\varphi}{\partial \theta^2}\right) \tag{7}$$

$$\frac{\partial U_r}{\partial r} + \frac{2U_r}{r} + \frac{1}{r}\frac{\partial U_\theta}{\partial \theta} = 0 \tag{8}$$

When the vehicle starts to move the flow of wind pass through the duct is proportional to the speed of the vehicle. The turbulent flow inside the converging duct will affect the boundary layer. The duct is designed in such a way that the maximum power attained with the speed of 60 km. If the vehicle speed increases an opposite force will be introduced. To avoid this problem an automatic valve mechanism is installed at the end of the duct. To estimate the boundary layer parameters different boundary condition has been considered. $U_r(r,\alpha) = U_\theta(r,\alpha) = U_\varphi(r,\alpha) = 0, U_r\left(r,\alpha-\beta_r r\right) = U_{rs}$, $\mathrm{U}_\varphi\left(r,\alpha-\beta_r r\right) = U_{\varphi s}$, $\mathrm{P}\left(\mathrm{r},\alpha-\beta\delta_{max} r\right) = P\beta_{\max}$, $\mathrm{U}_r(r_i,\theta) = U_{rn}$. To solve the above equations with boundary conditions the flow inside the duct is turbulent and the velocity profile is considered based on 1/n power distribution, here we are choosing n = 7 and U_r and M becomes, $U_r = U_{rs}\left(M/\beta_r\right)^{1/7}$ $M = r\left(\alpha-\theta\right)$. The axial velocity outside the boundary layer of wind duct can be calculated as

$$U_{\mathrm{ro}}\, 2\pi r^2\left(1-\cos\alpha\right) = \int_{\alpha-\beta_r r}^{\alpha} U_r r^2 \sin\theta d\theta d\varphi + U_r 2\pi r^2\left(1-\cos\alpha\right) \tag{9}$$

$$\frac{U_{rs}}{U_{ri}} = \left(\frac{r_i}{r}\right)^2\left(1+\frac{1}{8}\frac{\beta_r}{r\tan\alpha/2}\right) \tag{10}$$

Now the boundary layer momentum integral in the r direction can be determined from equation (5) and the value of sinè is very small so it is negligible.

$$\int_{\alpha-\beta_r r}^{\alpha} \frac{U_\theta}{r}\frac{\partial U_r}{\partial \theta} d\theta = \frac{1}{r}\int_{\alpha-\beta_r r}^{\alpha} U_r r^2 \sin\theta d\theta d\varphi + U_r 2\pi r^2\left(1-\cos\alpha\right) \tag{11}$$

The wall shear stress can be calculated directly from the relation used by Maddahian et al. [23]. The turbulent shear stress in the r direction is as follows:

$$\gamma_{r\theta} = 0.0225\rho U_r\left(\frac{U_r}{\beta_r}+\frac{U_\varphi}{\beta_\varphi}\right)^{2/3}\left(\frac{\nu}{\beta_r}\right)^{1/4} \tag{12}$$

4. UNSCENTED KALMAN FILTER

Most of the real time systems are nonlinear and it can be represented as discrete time system. Extended Kalman filer (EKF) is used to solve nonlinear problems. The transition matrix is consecutively changed

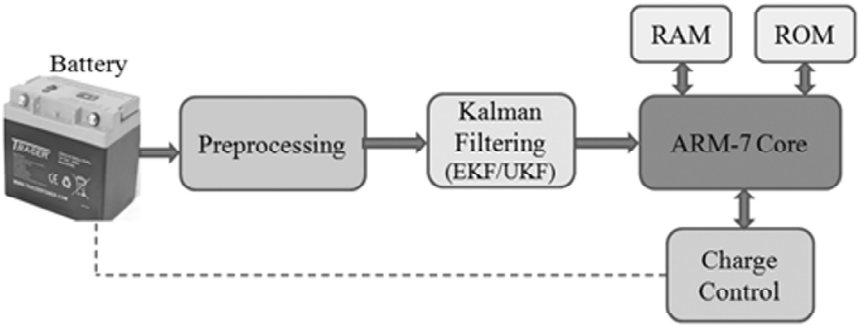

Figure 5: Measurement of SOC.

with respect to time. So it cannot be pre-computed and requires more computations. The battery charging controller (BCC) has the capability to estimate SOC, available power, and capacity under running condition. The algorithm has been implemented in a sodium chloride battery (Zebra) pack. The predicted function P_f and the updated function U_f are nonlinear practically. The EKF does not provide better performance in the non-linear system. The state of the battery is non linear. So that, the state space model may be non linear. The non-linear version of Kalman filter is called EKF and the summary is given in table 2. EKF linearizes the current mean and covariance of the system. The function f and h cannot be used to find the covariance directly. The previous estimation helps in calculating the predicted state. This non-linear model propagates covariance while doing linearization in EKF. So the performance of EKF is not up to the mark. The Unscented Kalman filter (UKF) utilizes more deterministic sampling points around the mean.

The mean and covariance can be estimated from the sample points used in the nonlinear function and it provides dynamic error bounds on these estimates. The advantages of this estimate are:

- The UKF estimation produces accurate results for different speed scenario of the EV.
- The temperature variation from 30° to 50° can be considered.

Table 2
Summary of EKF for SOC estimation.

Non linear state space model

$$X_k = f(X_{k-1}, U_{k-1}) + M_{k-1}$$

$$Z_k = h(X_k) + N_k$$

M_k and N_k are the system disturbance and observation noises which are assumed to be independent, zero mean, random white Gaussian processes with intensities W_k and V_k respectively.

Definition

$$F_{k-1} = \frac{\partial f(x_{k-1}, U_{k-1})}{\partial x_{k-1}} |_{x_{k-1} = \hat{x}_{k-1}}$$

$$H_k = \frac{\partial h(x_k, U_k)}{\partial x_k} |_{x_k = \hat{x}_k}$$

Initialization

For k=0, set $\hat{X}_0^+ = E[X_0]$, $\sum \hat{x}_0^+ = E\left[(X_0 - \hat{X}_0^+)(X_0 - \hat{X}_0^+)^T\right]$

Predict

Predicted state : $\hat{X}_{(k|k-1)} = f(\hat{X}_{k-1|k-1}, U_{k-1})$

Predicted covariance estimate : $C_{(k|k-1)} = F_{k-1} C_{k-1|k-1} F_{k-1}^T + M_{k-1}$

Update

measurement residual : $\tilde{y}_k = Z_k - h(\hat{X}_{k|k-1})$

residual covariance : $R_k = H_k C_{k|k-1} H_k^T + V_k$

Optimal Kalman gain : $G_k = C_{k|k-1} H_k^T R_k^{-1}$

Updated state estimate : $\hat{X}_{k|k} = \hat{X}_{k|k-1} + G_k \tilde{y}_k$

Updated covariance estimate : $C_{k|k} = (I - G_k H_k) C_{k|k-1}$

It uses $2k + 1$ sample points for k states instead of linearizing a nonlinear function. More deterministic sampling method used in UKF gives better performance and the algorithm is summarized in table 3. UKF is an easier method for calculating the statistics of a random variable to estimate SOC. This method undergoes a nonlinear transformation and builds on the principle that it approximates a probability distribution function. The measurement setup of SOC is shown in figure 5. The algorithm is combined with a cell model given in [22] to BCC functions. In the UKF method the real time estimation is done for different speed scenarios of EV. By applying Gaussian random variable in SOC estimation it will produce more instability in the output

Table 3
Summary of UKF algorithm for SOC estimation.

Predict

$$X^{v}_{k-1|k-1} = \left[\hat{X}^{T}_{k-1|k-1} \; E\left[M^{T}_{k}\right]\right]^{T}$$

$$C^{v}_{k-1|k-1} = \begin{bmatrix} P_{k-1|k-1} & 0 \\ 0 & W_k \end{bmatrix}$$

The state and covariance are combined with the weighted sampling point.

$$\hat{X}_{k|k-1} = \sum_{j=0}^{2L} Q^{j}_{s} \, X^{j}_{k|k-1}$$

$$C_{k|k-1} = \sum_{j=0}^{2L} Q^{j}_{c} \left[X^{j}_{k|k-1} - \hat{X}_{k|k-1}\right]\left[X^{j}_{k|k-1} - \hat{X}_{k|k-1}\right]^{T}$$

Where Q_c and Q_s are the weights of the covariance and state respectively.

$$Q^{0}_{s} = \frac{\mu}{L+\mu}, \; Q^{0}_{c} = \frac{\mu}{L+\mu} + (1 - \gamma^2 + \delta)$$

$$Q^{i}_{s} = Q^{i}_{c} = \frac{1}{2(L+\mu)} \text{ and } \mu = \gamma^2(L+k) - L$$

The sampling points which are controlled by k and V

Update

A set of sampling points 2L+1 are calculated as

$$X^{0}_{k|k-1} = X^{a}_{k|k-1}$$

$$X^{j}_{k|k-1} = X^{a}_{k|k-1} + \left(\sqrt{(L+\mu)}C^{a}_{k|k-1}\right)_{j}, \quad j = 1,2,\ldots L$$

$$X^{j}_{k|k-1} = X^{a}_{k|k-1} - \left(\sqrt{(L+\mu)}C^{a}_{k|k-1}\right)_{j-L}, \quad j = L+1,\ldots 2L$$

The sampling points are augmented in UKF prediction is

$$X_{k|k-1} := \left[X^{T}_{k|k-1} \; E\left[N^{T}_{k}\right]\right]^{T} \pm \sqrt{(L+\mu)}V^{a}_{k}$$

The observation function with the sampling point is as follows

$$\beta^{j}_{k} = h\left(X^{j}_{k|k-1}\right), \quad j = 0,1,2,\ldots 2L$$

The predicted measurement and covariance combining with the weighted sampling point is

$$\hat{z}_k = \sum_{j=0}^{2L} Q^{j}_{s} \, \beta^{j}_{k}$$

$$C_{zk=k} = \sum_{j=0}^{2L} Q^{j}_{c} \left[\beta^{j}_{k} - \hat{z}_k\right]\left[\beta^{j}_{k} - \hat{z}_k\right]^{T}$$

$$\text{Cross covariance} : C_{xx} = \sum_{j=0}^{2L} Q^{j}_{c} \left[X^{j}_{k|k-1} - \hat{X}_{k|k-1}\right]\left[\beta^{j}_{k} - \hat{z}_k\right]^{T}$$

$$\text{UKF gain} : G_k = C_{zk=k}C^{-1}_{xx}$$

$$\text{Updated covariance} : C_{k|k} = C_{k|k-1} - G_k C_{zk=k} G^{T}_{k}$$

because of linearizing the non-linear function. In UKF, $2L + 1$ sample points from L states are taken and pass through the non-linear function. In this case the random variable match with the mean and covariance and it will be recalculated. This approach reduces the computational complexities and increases the speed and accuracy of calculations.

The algorithm compares the voltage value predicted by Plett [22] with the measured cell voltage under running condition. In order to study the performance of UKF in SOC, we need to verify the pulse power capability using hybrid pulse power characterization (HPPC) described in [20]. HPPC is used to estimate the dynamic power capability over the voltage and charge range of the battery. A test profile of HPPC characterization is shown in figure 6. It shows that the discharge and charge pulse power capability at different depth of discharge (DOD) values. For estimating SOC, the cell was initially fully charged. The charge and discharge pulse range were used form 100A to 1A.

5. RESULT AND DISCUSSION

The rectangular duct is placed on the top of the electric vehicle. The turbulent flow in a convergent rectangular duct with inlet mouth size of 1meter length and 0.5 meter height, and the outlet mouth size of 0.4m length, 0.2m height and inlet velocity ratio of 0.6 are chosen. If vehicle moves, velocity near the duct inlet will vary, as a result the frictional and wall effects penetrate into the flow depends on the inlet velocity.

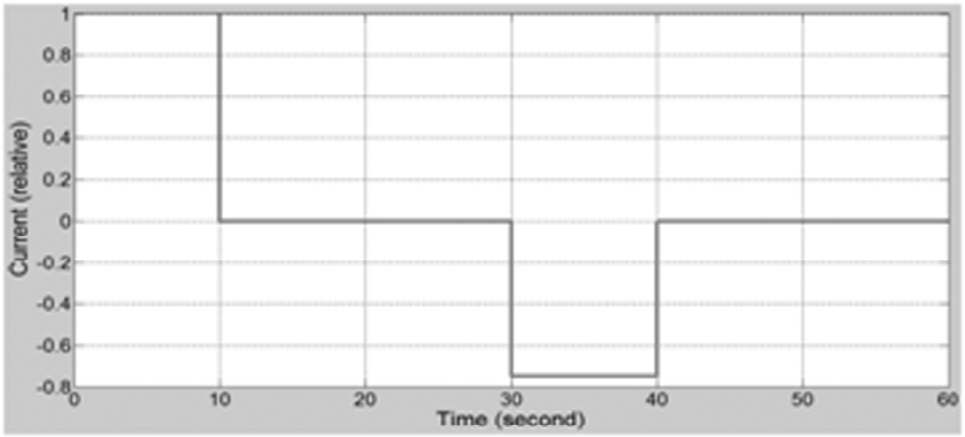

Figure 6: Test profile of HPPC characterization.

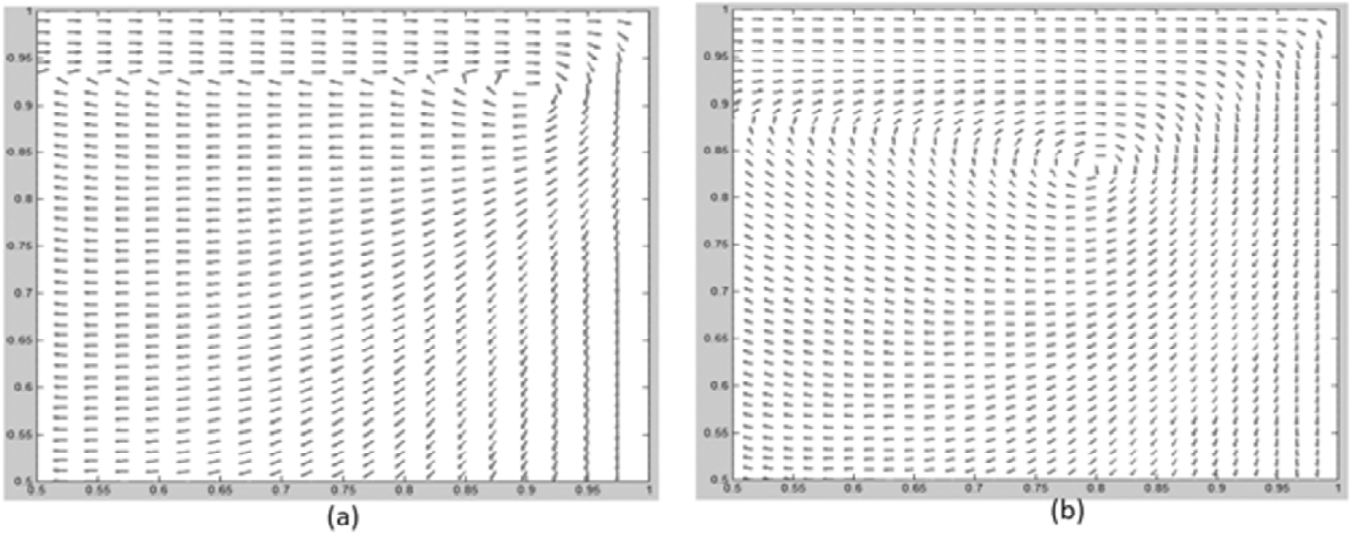

Figure 7: Navier-Stokes velocity vector and duct angle (a) 10 degree (b) 20 degree.

The boundary layer thickness of rectangular duct will vary with duct angle. If the duct angle increases, both the rotational and axial velocities increases and the thickness of both the axial and rotational boundary layer gets decreases. On the other hand, if we increase the duct angle the location of boundary layer thickness moves towards the mouth of the rectangular duct. Figure 7 shows the velocity vector for two different duct angles. Figure 7(a) shows the velocity vector of 10^o duct angle and it has more separation and figure 7(b) shows the velocity vector of 20^o duct angle and it has attached flow. Figure 8 shows the boundary layer thickness for different duct angle in the rotational and axial directions. Figure 8(a) depicts that if the duct angle increases the boundary layer thickness decreases gradually.

Figure 8(b) shows the boundary layer thickness for different duct angle in the rotational direction. The figure depicts that if the duct angle increases the boundary layer thickness decreases gradually. Comparing the axial and rotational boundary layer thickness, the rotational boundary layer has higher thickness range than axial boundary layer for the same duct angle.

The shear stress, angle of duct, and the boundary layer are closely related to each other. If the boundary layer thickness is higher, then the shear stress of wall decreases gradually. Figure 9 shows the shear stress of duct wall for various angles. The inlet velocity of rectangular duct increases if the speed of vehicle increases. Figure 9(a) shows the shear stress of rotational direction and it decreases gradually if duct angle increases. On the other hand, the increase in inlet velocity automatically increases the streamline flow along the rotational and axial direction as a result increases of shear stress. Figure 9(b) shows the shear stress of axial direction,

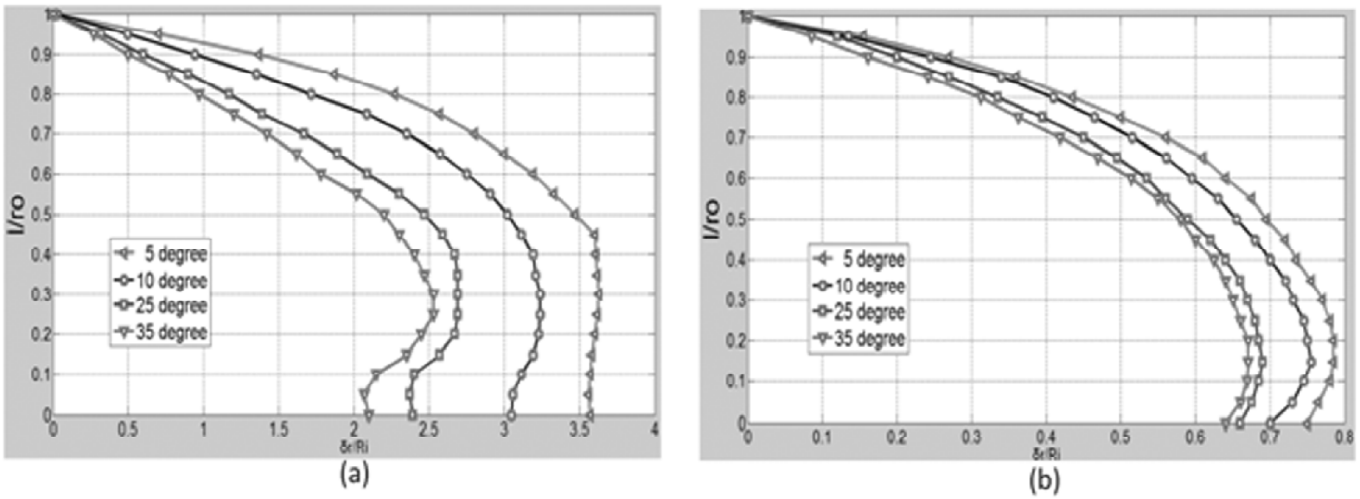

Figure 8: Effect of duct angle on boundary layer thickness (a) rotational (b) axial.

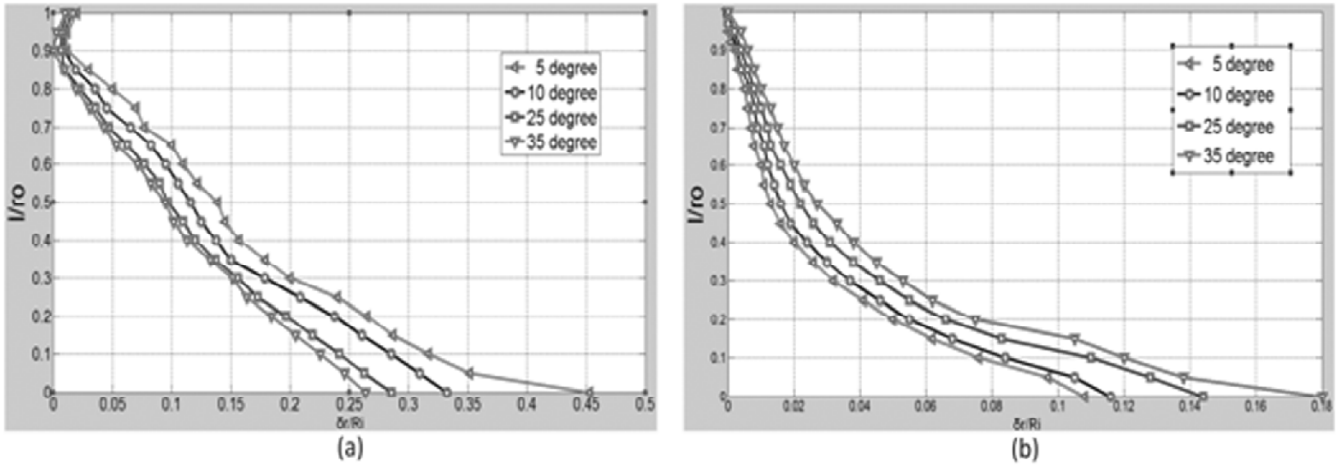

Figure 9: Effect of duct angle on shear stress (a) rotational (b) axial.

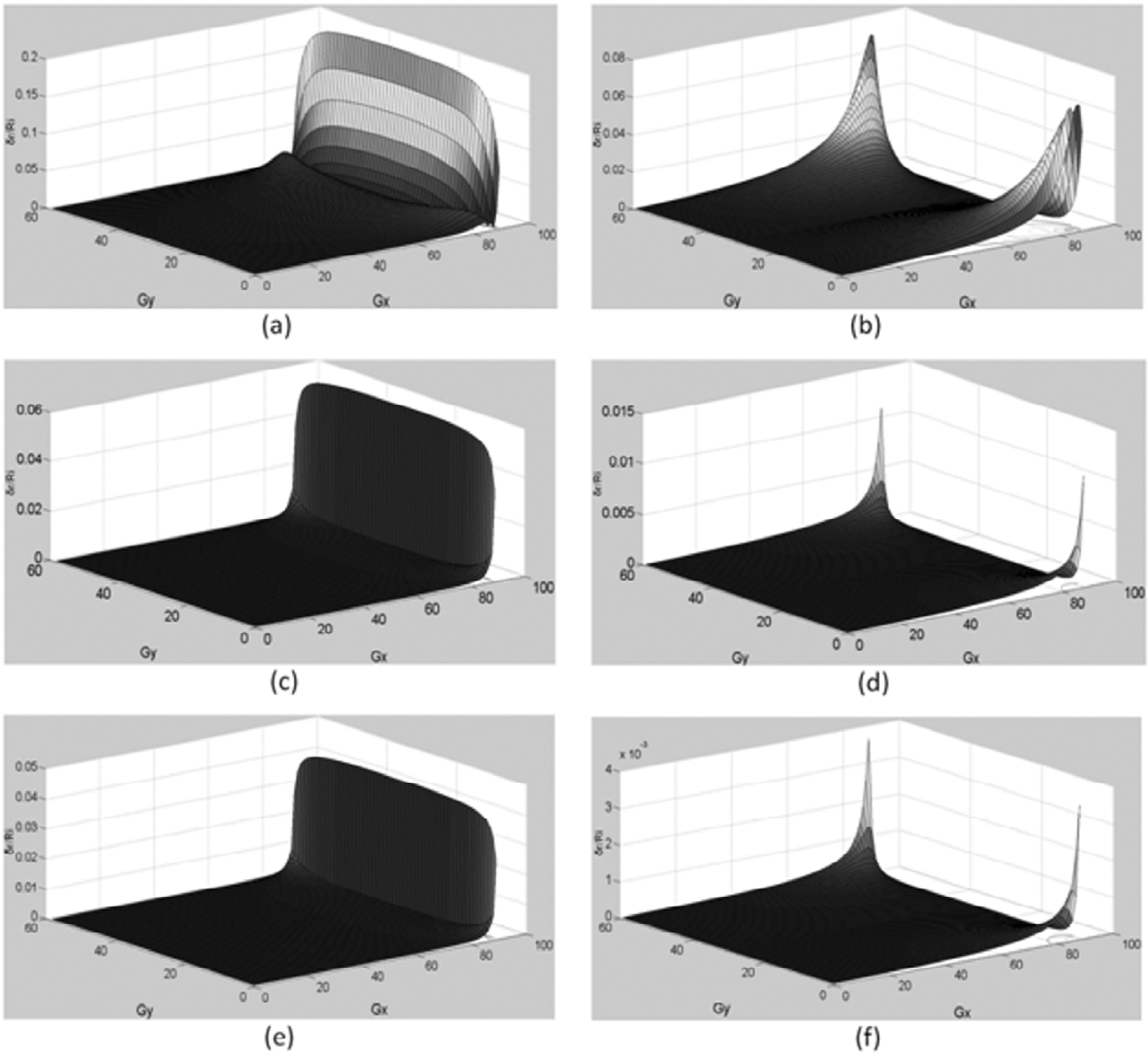

Figure 10: Effect of RN on boundary layer thickness: (a, c, e) rotational, (b, d, f) axial.

decreases gradually if duct angle increases. On comparing both the rotational and axial shear stress the rotational stress is greater than axial shear stress. The shear stress is less in the mouth of the duct.

The velocity of inlet varies depends on the speed of vehicle. To study the effect of RN we considered the speed of vehicle is constant and estimates the boundary layer for various values of RN. Figure 10 shows the effect of RN on rotational and axial boundary layer. We calculated the boundary layer for three different values: RN = 1×10^3, 2×10^4, and 5x105. Figure 10(a),(c),(e) shows the rotational boundary layer thickness for different values of RN and figure. 10(b),(d),(f) shows the axial boundary layer thickness and it depicts that if RN increases the boundary layer thickness decreases. Comparing both the rotational and axial boundary layer thickness for all the three cases of RN, the axial boundary layer thickness is smaller than the thickness of rotational boundary layer.

Three different speed scenarios are considered for SOC error estimation compared with both the EKF and UKF. Pulsed current test was taken and the performance is carried out. The following assumptions are made for this estimation.

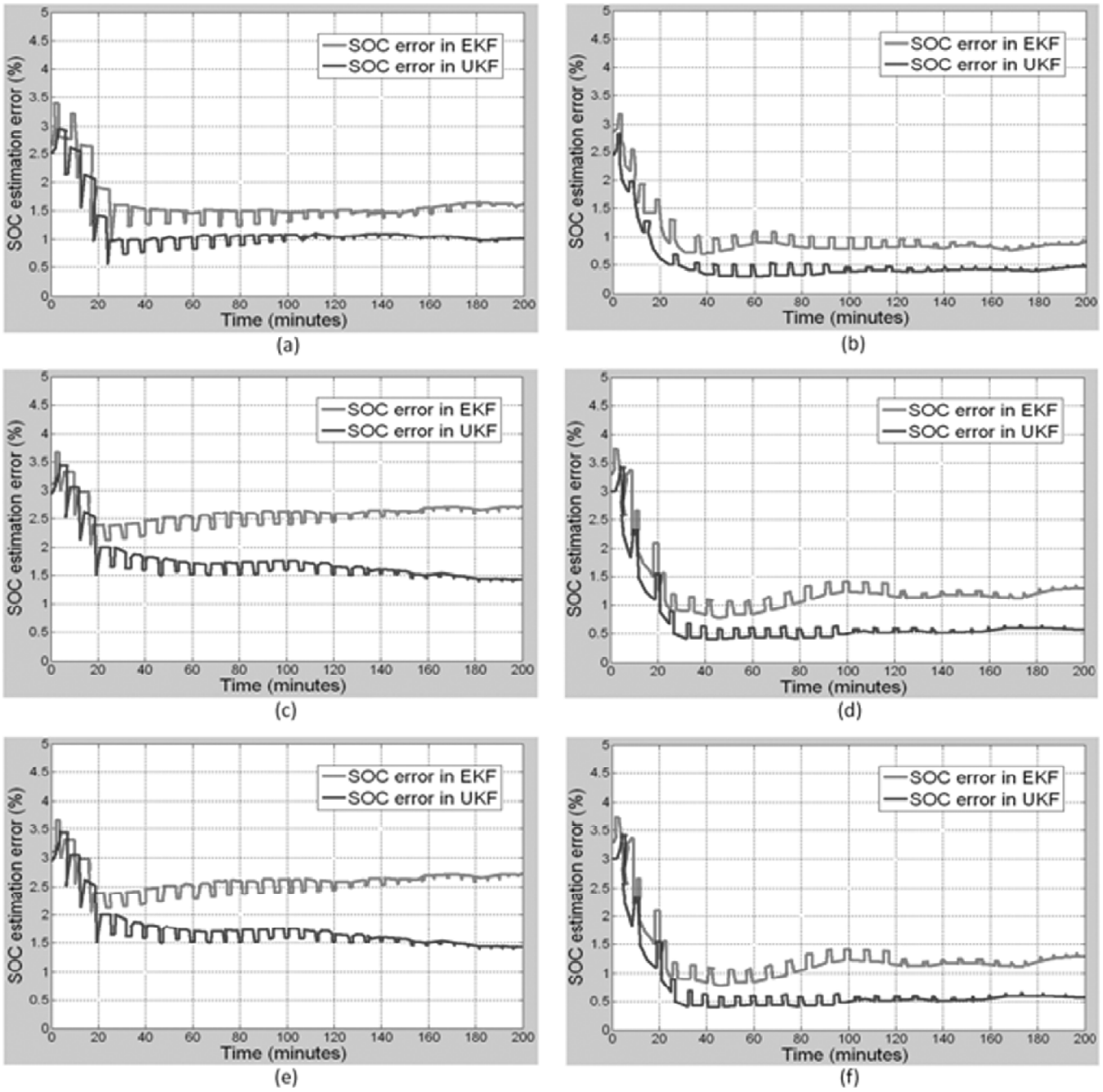

Figure 11: Error during SOC estimation using EKF and UKF for HPPC cell test: (a, b) 0-20 km speed, (c, d) = 21-40 km speed, (e, f) 41-60 km speed.

- The state estimation model and system model are same.
- Both the process and measurement noise are considered and Gaussian noise is applied.
- The covariance of both the process and measurement noise is same for EKF and UKF.
- The sampling frequency is same as that of the measurement frequency.
- In UKF algorithm the following values are considered. $\mu = 0.1$, $\delta = 2$, $k = 0$

SOC estimation using EKF and UKF for pulsed current test is shown in figure 11. The figure illustrates the error estimation of both the charging and discharging of battery system connected to GEH. In figure 11(a),(c), (e) shows the error estimation under charging the battery for 20 km, 40 km, and 60 km speed

respectively. Figure 11(b),(d),(f) shows that the error estimation under discharging of battery for 20 km, 40 km, and 60 km speed respectively. The UKF estimation starts with zero for all the three speed scenarios. Figure 11(a) and (b) shows that the error estimation with the speed ranges from 0-20 km. In this case both the charging and discharging rate is almost equal. Figure 11(c) and (d) shows that the error estimation with the speed ranges from 21-40 km. The percentage of error is greater than that of first case. Compared to EKF the error rate of UKF is less in SOC error estimation. In figure 11(e) and (f) describes the error estimation with the speed range from 41-60 km. In this case the charging rate is greater than that of discharging rate. Compared to all the three speed scenarios UKF produces less error rate than EKF. From the output we can conclude that UKF estimation is better than that of EKF. The percentage of error is less than 2% in UKF and greater than 3% in KEF under 60 km speed scenario and it is less than 2% in lower speed scenario. The charging and discharging takes place simultaneously and the charging portion of the pulse current test follow the discharge according to the speed of the vehicle. In this state the rate of discharge is greater than the rate of charge.

The capacity delivery of the battery depends on the rate of discharge as well as battery temperature. Figure 12 shows the depth of discharge for three different speed scenarios for 30 minutes running time of EV. The two ellipses indicate that the EVs are incorporated with and without GEH respectively. The curves

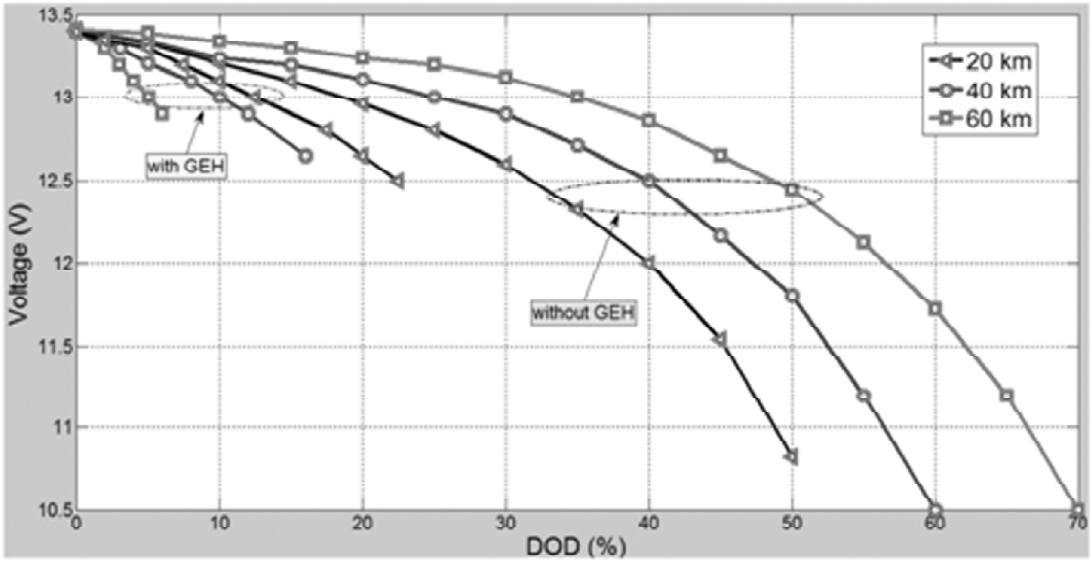

Figure 12: Discharge curve at various speeds.

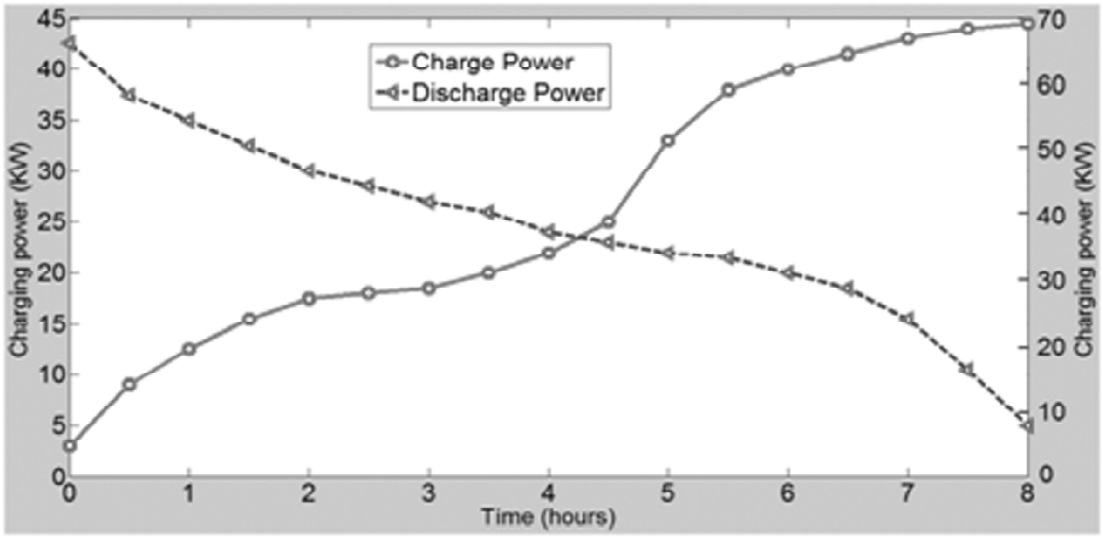

Figure 13: HPPC cell test for charge and discharge power

under right side ellipse are not connected to GEH and it shows the rate of DOD for three different speed scenarios. If speed increases the rate of DOD is also increases. In the case of 20 km speed the DOD is around 53% and at 60 km speed it is around 70%. The voltage is reduced to 10.5-11 volts for all the speed scenarios. On the other hand the curves under the left side ellipse are connected to GEH for three different speed scenarios. If speed increases, the DOD decreases because maximum voltage will be produced by the generator at the speed of 60 km. In this case, for 20 km speed the DOD is around 22% and it is around 6% for 60 km speed. For all the cases the voltage range is 12.5 volts. So that the SOC of battery is increased at high-speed scenario compared to a low speed.

From figure 12 we can easily understand that recharging is needed for hour duration but GEH does not require such type of recharging. The voltage range can be maintained between 12.5V and 13V. Moreover the rate of charge is also depends upon the capacity of harvesting system we incorporated. The power versus energy data for HPPC cell test is shown in figure 13. Here the charging and discharging powers are taken as y-axis and the time is taken as x-axis for easy comparison of both the results. From this output we can understand that the charging power equalizes the discharging power and the SOC will be maintained in GEH.

According to table 1 we calculated the traveling distance for 10 hours duration is shown in figure 14. From the graph we can understand that the proposed EV covers three times greater distance as the ratio 1:3. So we strongly say that the proposed method will increase the usage of EVs and create the way for green environment.

6. CONCLUSION

In this paper we have presented a new charging scheme for EVs to reduce the travelling time and thereby to increase the usage of EVs. The traveling time depends on the capacity of the battery pack present in the vehicle. The countries, which use EV, provide recharging facility for EVs and this leads to increase in travelling time. The proposed method provides solution for this problem. In this study we analyzed both the performance of wind duct and SOC of battery packs. For analyzing the performance of wind duct three different scenarios have taken. We are not considered other losses at the running time of vehicle. The numerical analysis of wind duct shows that the axial and rotational boundary layer thickness depends on the velocity ratio, Reynolds number, and the angle of rectangular duct. The boundary layer thickness will decrease if RN increases. The shear stress also depends on the angle of duct. We have estimated the performance of battery packs using both the EKF and UKF. We used HPPC test profile to estimate the dynamic power of the battery pack over the charge and voltage range. From the performance comparison

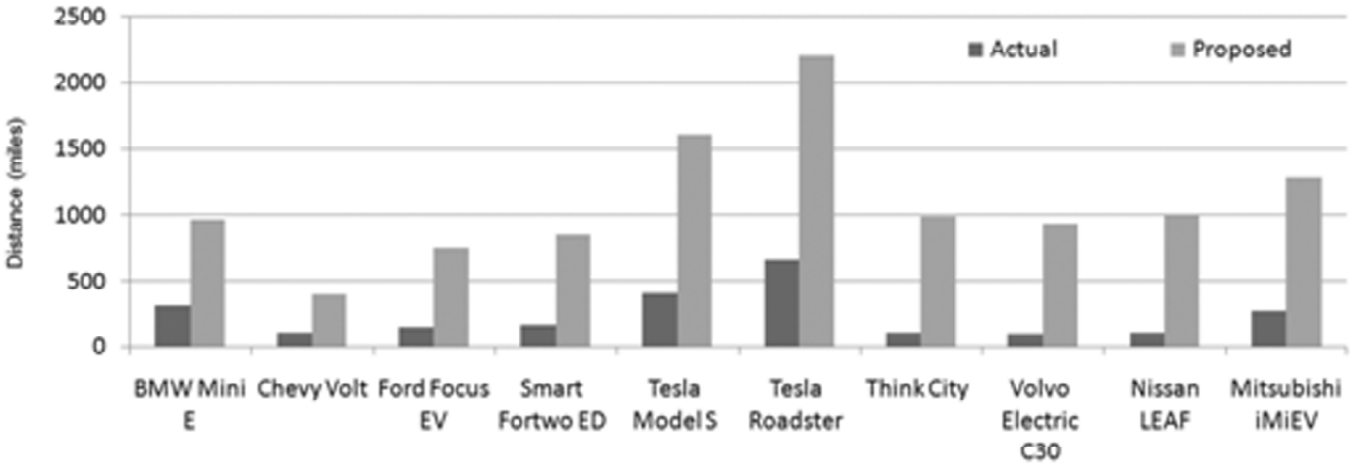

Figure 14: Comparison of traveling distance for various EVs.

we can conclude that the UKF produce less error than EKF and it can accurately estimates the available power. The discharging rate of EV for three different speed scenarios with and without GEH has been studied. The EV with GEH has less discharging rate because it automatically recharges the battery packs while running. The DOD is around 22% and the voltage is 12.5 V for 20 km, DOD is 16% and the cell voltage is 12.8 V for 40 km, and DOD is around 6% and the voltage is 13.2 V for 60 km speed. Finally we conclude that this approach reduces the total traveling time and increase EVs as a result creating pollution free environment. The authors believe that the implemented system has many advantages and can adopt by developing countries at all levels.

REFERENCES

[1] Chellaswamy Chellaiah, Balaji. T.S., Muhuntharaj. C., "Design of a Fuel Free Electric Vehicle Using Fuzzy Logic for Pollution Control."*International Conference on Modeling Optimization and Computing*, *Proceedia Engineering*, volume 38, pp. 1547-1558, 2012.

[2] Damien Biau, Houssam Soueid, Alessandro Bottaro., "Transition to Turbulence in Duct flow."*Journal of Fluid Mechanics*. Volume 596, pp. 133-142, 2008.

[3] Eckhardt B., Schneider T. M., Hof B., Westerweel J., "Turbulence transition in pipe flow."*Annual Review of Fluid Mechanics*, pp. 447–468, 2007.

[4] Federico Millo, Luciano Rolando, Rocco Fuso, Fabio Mallamo.,"Real CO2 Emissions Benefits and End User's Operating Costs of a Plug-in Hybrid Electric Vehicle." *Applied Energy*, pp. 563-571. 2014.

[5] Fue-Sang Lien, Eugene Yee., "Numerical modelling of The Turbulent flow Developing within and Over a 3-D Building Array, Part I: A High-Resolution Reynolds-Averaged Navier–Stokes Approach."*Boundary-Layer Meteorology*, pp. 427–466, 2004.

[6] Freedom CAR Battery Test Manual for Power-Assist Hybrid Electric Vehicles. 2003.

[7] G. Plett., "Extended Kalman Filtering for Battery Management Syatems of LiPB Based HEV Battery Packs Part: 2 Moddelling and identification."*Journal of Power Source*, Volume 134, pp. 262-276, 2004.

[8] Gianmario Pellegrino, Eric Armando, Paolo Guglielmi., "An Integral Battery Charger With Power Factor Correction for Electric Scooter." *IEEE Transactions on Power Electronics*, pp. 751-759, 2010.

[9] Kanellos. F D., "Optimal Power Management With GHG Emissions Limitation in All-Electric Ship Power Systems Comprising Energy Storage Systems."*IEEE Transactions on Power Systems*, pp. 330-339, 2014.

[10] Laxman Maharjan, Shigenori Inoue, Hirofumi Akagi, Jun Asakura., "State-of-Charge (SOC)-Balancing Control of a Battery Energy Storage System Based on a Cascade PWM Converter."*IEEE Transactions on Power Electronics*, 1628-1636, 2009.

[11] Man Ho Au, Joseph K Liu, Junbin Fang, Zoe L Jiang, Willy Susilo, Jianying Zhou., "A New Payment System for Enhancing Location Privacy of Electric Vehicles." *IEEE Transactions on Vehicular Technology*, pp. 3-18, 2014.

[12] Mosaddek Hossain Kamal Tushar, Chadi Assi, Martin Maier, Mohammad Faisal Uddin., "Smart Microgrids: Optimal Joint Scheduling for Electric Vehicles and Home Appliances, *IEEE Transactions on Smartgrid*, pp. 239-250, 2014.

[13] Maddahian R., Kebriaee A., Farhanieh B., Firoozabadi B., "Analytical investigation of boundary layer growth and swirl intensity decay rate in a pipe." *Archive of Applied Mechanics*, Volume 81, Issue 4, pp. 489–501, 2010.

[14] Pathuri Bhuvana V., C. Unterrieder, J. Fischer., "Battery Internal State Estimation: Simulation Based Analysis on EKF and Auxiliary PF." *EUROCAST-2013*, pp. 469–475, 2013.

[15] Rambabu Kandepu, Bjarne Foss, Lars Imsland., "Applying the unscented Kalman filter for nonlinear state estimation." *Journal of Process Control*, Volume 18, pp. 753-768, 2008.

[16] Rudolph Van Der Merwe., "Sigma-Point Kalman Filters for Probabilistic Inference in Dynamic State-Space Models, Dissertation."*Electrical and Computer Engineering*, *Oregon Health and Science University*, 2004.

[17] Sridhar Ungarala, Eric Dolence, Keyu Li., "Constrained Extended Kalman Filter for Nonlinear State Estimation."*8th International IFAC Symposium on Dynamics and Control of Process Systems*, 2007.

[18] Simon J Julier, Jeffrey K. Uhlmann., "Unscented Filtering and Nonlinear Estimation."*Proceedings of the IEEE*, pp. 401-422, 2004.

[19] Shalman, F., A. Yakhot, S. Shalman, O. Igra, Y. Yadlin., "Attenuating Artificial Dissipation in the Computation of Navier-Stokes Turbulent Boundary Layers," *Journal of Scientific Computing*, Volume 13, Issue 2, pp. 151-172, 1998.

[20] Schlichting, H., Boundary Layer Theory. 7th ed. McGraw-Hill. New York, 1973.

[21] Thomas Y. Hou, Congming Li., "Dynamic Stability of The Three-Dimensional Axisymmetric Navier-Stokes Equations With Swirl." *Communications on Pure and Applied Mathematics*, LXI, pp. 0661–0697, 2008.

[22] Tan Ma, Osama Mohammed., "Optimal Charging of Plug-in Electric Vehicles for a Car Park Infrastructure." *IEEE Transactions on Industry Applications*, pp. 1-8, 2012.

[23] Wade P. Malcolm, Caroline J. Narich, Mark Schutz., "Plug-in electric vehicles Changing perceptions, hedging bets, *Accenture end-consumer survey on the electrification of private transport*, 2011.

[24] Xiao song HU, Feng chun SUN, Xi ming Cheng., "Recursive Calibration for a Lithium ion Phosphate Battery for Electric Vehicle Using Extended Kalman Filtering."*Journal of Zhejiang University-Science A (applied physics and Engineering)*, pp. 818-825, 2011.

[25] Xiong, R., F. C. Sun, H. W. He., "Data-Driven State-of-Charge Estimator for Electric Vehicles Battery Using Robust Extended Kalman Filter." *International Journal of Automotive Technology,* 15, 89-96, 2014.

[26] Zhihao Yu, Ruituo Huai and Linjing Xiao., "State-of-Charge Estimation for Lithium-Ion Batteries Using a Kalman Filter Based on Local Linearization." *Energies*, Volume 8, pp. 7854-7873, 2015.